Proceedings of the International Conference on Heat Exchanger Fouling and Cleaning - 2024 (Peer-reviewed)
April 21–26, 2024, Lisbon, Portugal; Editors: H.U. Zettler and E.M. Ishiyama

HYDRAULIC AND THERMAL DEVELOPMENT OF FOULING LAYER

***E. Crosby, M. Berger, B. Houston, and L. Bishop**
Heat Transfer Research, Inc., P.O. Box 3290, Navasota, TX 77868, elijah.crosby@htri.net

ABSTRACT

Industrial cooling water fouling is the undesired formation of deposits on heat transfer surfaces. This deposition increases the hydraulic and thermal resistances of a heat exchanger and negatively affects its performance. This paper describes HTRI's mobile skid-mounted unit and presents test results using two water sources. The unit allows direct comparison of cooling water fouling in two different tubes in an identical environment. The analysis uses two approaches to determine fouling resistances: one, the change in overall resistance and two, the change in heat transfer resistances of the cooling and heating media because of the deposit. Finally, results of river water tests are highlighted, clearly showing thermal fouling resistance trends compared with pressure drop profiles. These data suggest that, in certain cooling water fouling situations, hydraulic constraints outweigh thermal degradation and flow distribution can become a concern with cooling water system networks.

INTRODUCTION

HTRI's cooling water fouling test rig enables comparison of tubeside fouling for a pair of test sections in a shared heat transfer environment. The test rig is designed to operate close to common industry cooling water conditions and is compatible with a range of water chemistries, supporting realistic evaluations of the fouling propensity of various tube enhancements, coatings, and metallurgies. This paper describes the process of collecting and analyzing fouling data in the test unit. It then presents a subset of recent test data to illustrate unexpected results that need further investigation. Lastly, it discusses data analysis from a fundamental fluid mechanics viewpoint and describes the effects and modeling of fouling layer growth from both the hydraulic and thermal perspective.

MATERIALS AND METHODS

HTRI's mobile cooling water fouling test unit produces a shared fouling environment for two test sections that isolates the tubeside condition as the differentiating factor. This enables direct comparison and easier evaluation of an enhancement or fouling mitigation strategy. The unit is self-contained and can operate with a single 220V 50-amp plug.

As shown in Fig. 1, the cooling water flow starts from the test fluid tank, moves through the pump, and then splits into two separate flow paths before entering the test section, a 203.2-mm shell with two side-by-side 12.7-mm tubes running along the top of the shell. Inside the test section, two submerged electric heaters evaporate water in the bottom of the shell. The evaporated water rises over the two tubes, condenses, and then falls to the bottom of the shell to be re-evaporated.

The cooling water gains heat by this process and then exits the test section to enter an air cooler, where the amount of heat rejected varies according to the speed of fan. The fluid then returns to the tank.

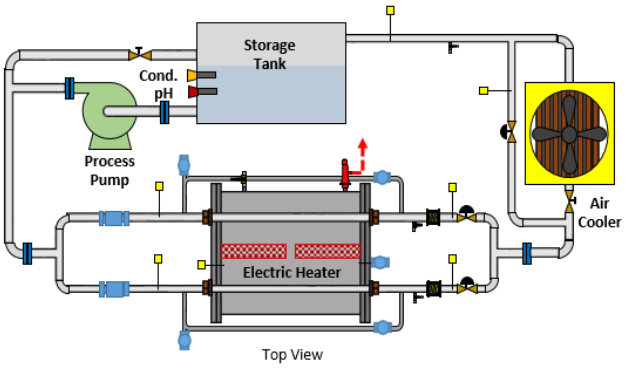

Fig. 1. Process flow diagram.

The test water conductivity and pH are measured in the tank. Test section inlet/outlet temperature and pressure drop are monitored, as are the heater power and shell steam temperature. Control measurements after the air cooler control the fan speed so that the test section water reaches the desired inlet temperature.

The side-by-side configuration of the test section tubes allows any internal enhancement, different metallurgies, and coatings to be tested against a plain tube. The unit also enables a

ISBN: 978-0-9984188-3-4; Published online www.heatexchanger-fouling.com

comparison between velocities or Reynolds numbers. However, the current configuration does not allow direct change of the heat flux or inlet temperature for each tube.

Fig. 2 Cooling water fouling unit

A cutaway view of the test section layout (Fig. 3) shows the shellside process along with the tube configuration. The unique design of the unit allows either a constant shell pressure test, where the shellside pressure is maintained at the initial level throughout the entire test when fouling occurs, or a constant heater power test, where the heater power is set and maintained throughout the entirety of the test. The constant pressure test with the addition of a fouling resistance allows the interface temperature of the fouling layer to vary. The constant power test ensures that the heat flux is always maintained, keeping the fouling interface temperature much closer to a constant value. Both operation test modes are industrially relevant, providing insights into fouling layer growth and cooling water fouling asymptotes. Both modes have been tested, with the constant pressure resulting in a lower fouling resistance, as expected due to the decline of the interface temperature of the fouling layer [1].

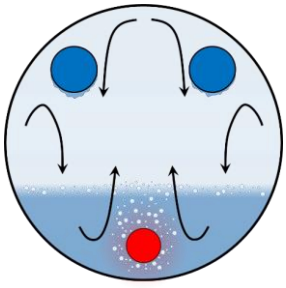

Fig. 3. Test section shell front view of test tubes and electric heater

TEST PROCEDURE

Fouling tests on the unit start with a pressure test to ensure that the unit is airtight, as the condensing shellside steam is under vacuum and leaks into the system have a large effect on the shellside heat transfer. After the pressure test, a baseline test is run that mimics the changing tubeside resistance to accurately correlate the shellside heat transfer coefficient. This is done by dropping the tubeside flowrate, thus simulating the change in tubeside resistance that occurs with a fouling layer present. With the pressure and baseline tests complete and performance verified, the fouling test is then run.

Baseline Test

After pressure testing, the baseline test is started. Each condition in the baseline test matrix (cooling water velocity, inlet temperature, and shellside heater power) is controlled for a certain time to ensure steady state conditions. The data are recorded for analysis to create the trend for the shellside heat transfer coefficient during fouling. Fouling occurs only on the tube side of the test section. In the baseline test, simulating the increased thermal resistance of the fouling layer means changing the tubeside heat transfer coefficient through manipulation of flow rate and temperature.

The tubeside heat transfer coefficient is calculated using HTRI's proprietary constants in the Dittus-Boelter correlation along with the Sieder-Tate correction, defined by Equation (1) [2]. Note that constants from literature are available with acceptable accuracy as well.

$$\mathrm{Nu}_i = C\left[\mathrm{Re}^a\,\mathrm{Pr}^b\left(\frac{\mu}{\mu_w}\right)^n\right] \tag{1}$$

The tubeside velocity, inlet temperature, and shellside heater power are changed to achieve different shellside pressures and heat transfer coefficients for the shellside correlation.

With the baseline test completed, the shellside heat transfer coefficient is calculated using the overall resistance concept of Equations (2) – (4).

$$\frac{1}{h_o} = \frac{1}{U_o} - \frac{1}{h_i}\left(\frac{D_o}{D_i}\right) - R_w \tag{2}$$

$$U_o = \frac{Q}{A_o LMTD} \tag{3}$$

$$R_w = \frac{D_o \ln\left(\frac{D_o}{D_i}\right)}{2k} \tag{4}$$

Fouling Test

Following baseline tests, the test fluid (for these tests, either Navasota River or city water) is loaded and a sample pulled for water chemistry analysis. Vacuum is re-established and maintained throughout the fouling test, and the conditions for

ISBN: 978-0-9984188-3-4; Published online www.heatexchanger-fouling.com

the fouling test are set and maintained. Conditions are monitored until either the shellside pressure, temperature, or power no longer change, indicating that a thermal fouling asymptote has been reached. No modifications to the water chemistry are made during a test, although future tests may allow for that to be done.

During testing, water conductivity, pH, pressure drop, flow rate, inlet/outlet temperatures, shellside temperature and pressure, and heater power are continuously monitored. Additionally, testing start/end water samples are taken and sent to an external lab for analysis. Throughout testing, HTRI takes and tests internal samples to track the change in water quality over time. The water fouling test rig is a closed loop system, so any changes in conductivity or pH, depending on the type of fouling occurring, correspond to a change in the chemical makeup of the water as deposits thicken on the test section. Fouling effects comprised of chemistry, thermal, and hydraulic contributions can be tracked.

After a test is completed, the heater is shut off and the unit allowed to cool down under a reduced flow rate. When ambient conditions are reached, the test section shellside pressure is used to calculate the amount of air in the system, confirming that no leaks have occurred. The tubes are then removed and cut open. The fouling layer is visually examined and then scanned with a microscope. Visual examination and evaluation under the microscope provide useful characterization of the fouling distribution, thickness, and roughness.

DATA EXAMINATION

Two methods are used to estimate the thermal fouling resistance obtained from fouling tests. The first approach is to calculate and trend the change in the overall heat transfer resistance of the tube. The change is measured from an initial point after startup is complete and steady state has been achieved. The initial overall heat transfer resistance is chosen as the reference resistance, and any change in this resistance is considered a fouling resistance. This approach is given in Equation (5).

$$R_{f,u}(t) = \frac{1}{U_o(t)} - R_{initial} \tag{5}$$

This basic approach bundles all fouling changes into a single fouling resistance term [3].

The second approach is to use the overall resistance with the shellside and tubeside convective coefficients calculated throughout the fouling period, as shown in Equation (6).

$$R_f(t) = \left[\frac{1}{U_o(t)} - \frac{1}{h_o(t)} - \frac{D_o \ln\left(\frac{D_o}{D_i}\right)}{2k} - \frac{1}{h_i(t)}\left(\frac{D_o}{D_i}\right) \right] - R_{initial} \tag{6}$$

This paper focuses on the second approach in calculating the fouling resistance.

The hydraulic analysis involves plotting the pressure drop over the testing time. Any increase in pressure drop is due to either a roughening of the heat transfer surface or to a constriction in the flow. Conductivity and pH plots help corroborate the thermal fouling resistance trend and provide further support for the type of fouling (i.e., particulate, crystallization, chemical reaction, corrosion, or biological) observed, as well as why asymptotes have been reached.

RESULTS AND DISCUSSION

This paper presents two tests with river and city water at an inlet temperature of 46.1 °C and tubes of copper-nickel. Table 1 provides further details of the test conditions. Both tests contain tubes with flow at different velocities, highlighting the ability of the rig to compare tubes side-by-side. A comparison for the reduction of fouling at a higher velocity can be made utilizing this rig.

Table 1. Fouling test conditions

Test	1	2
Water	City	River
Tube material	90-10 Cu-Ni	90-10 Cu-Ni
Heat control	Constant Heat Flux	Constant Heat Flux
Inlet tube temperature, °C	46.1	46.1
Velocity, tube 1, m/s	2	2
Velocity, tube 2, m/s	1	1
Heat flux, kW/m^2	65	65

The fouling trends of each test are shown in Fig. 4 and Fig. 5. The first graphs in each figure show a trend of the fouling resistance of each test tube vs. time. The second graph plots pressure drop across the length of the heated portion of the tube for each test tube vs. time. The third graph characterizes both the pH and conductivity of the closed loop tubeside water vs. time. Each of these trends illustrates a fouling layer buildup over time that increases thermal and hydraulic resistance. The chemical changes confirm the fouling layer growth: as conductivity (directly linked to the amount of dissolved solids in the water) drops, the thermal and hydraulic resistances increase.

The rest of this paper explores specific test results in more detail, including interpretations of the link between thermal and hydraulic fouling

ISBN: 978-0-9984188-3-4; Published online www.heatexchanger-fouling.com

resistances with chemistry changes considered. A close review of the test results shows that the thermal, hydraulic, and chemical changes of the water do not always align with expectations.

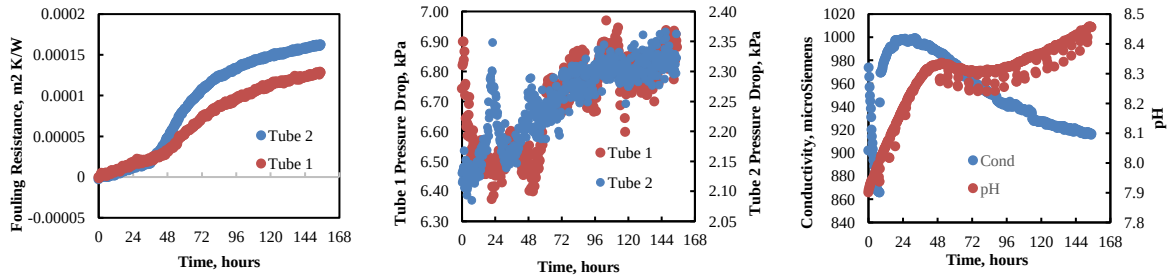

Fig. 4. Test 1 (city water) thermal (a), hydraulic (b), and chemical (c) fouling trends.

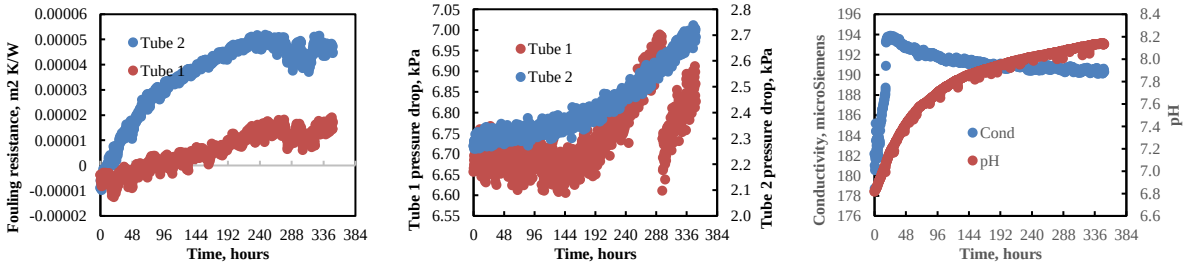

Fig. 5. Test 2 (river water) thermal (a), hydraulic (b), and chemical (c) fouling trends.

What is observed is the following:

- Test 1 (with Navasota city water) shows increasing pressure drop and thermal fouling resistance trends, as both parameters approach asymptotes at approximately the same time. While the conductivity decreases with time, it also approaches an asymptote at a similar period as both the pressure drop and thermal resistance parameters. Via X-ray diffraction analysis, the dominant mechanism was determined to be crystallization.
- Test 2 (with Navasota River water) shows that the pressure drop, thermal fouling resistance, and conductivity do not agree with other test trends. The conductivity does not asymptote at the same time as the fouling resistance, nor does the pressure drop. The pressure drop continues rising well after the fouling resistance has reached an asymptote. The primary fouling mechanism here is particulate, with no induction time observed.
- In each test, an initial linear or quasi-linear thermal fouling rate is followed by a reduction in this rate over time and then an asymptote. Despite different fouling mechanisms, these trend characteristics are similar.

The fouling layer in tests with city water does not totally cover the entire heat transfer area of the tube with 2 m/s flow, while that in tests with river water does cover the entirety of each tube. An important parameter to consider along with the fouling layer *thickness* is the fouling layer *coverage* [4].

The fouling layer builds up unevenly. The layer thickness is not the same throughout the heat transfer area but varies according to the wall temperature, typically being at its thickest at the hottest end of the tube and its thinnest (or even nonexistent) at the coolest end. Hence, the thermal and hydraulic resistances are averages of the overall effect of the fouling layer and not representative of the fouling layer itself. The "simplified" estimate of deposit resistance is given in Equation (7) [4].

$$R_d = \frac{\delta_{d,avg}}{k_d} \tag{7}$$

As the deposit builds up unevenly, the actual deposit resistance can be thought of in terms of the clean vs. fouled areas, that is, as a parallel thermal resistance network:

$$\frac{1}{R_d} = \frac{1}{R_{clean}} + \frac{1}{R_f} \tag{8}$$

A fouling thermal asymptote can be reached even if the deposit thickness growth continues in a localized region of the heated area of the tube. Thus, reaching a fouling asymptote may follow one of two possible routes:

- The fouling layer stops increasing in thickness
- The fouling layer stops spreading over the tube

An uneven fouling layer distribution can have a different impact on the pressure drop than on the heat transfer, depending on the overall deposition distribution and roughness.

ISBN: 978-0-9984188-3-4; Published online www.heatexchanger-fouling.com

Another point to consider is that the fouling layer is porous [5]. The density and thermal conductivity of measured fouling layers do not correspond to the density and thermal conductivity of the foulant material, but rather to a mixture of water and foulant, with a certain porosity changing the assumed values of thermal conductivity and density. Thus, a fouling layer thickness cannot be assumed to be obtained by the mass of the material deposited divided by the density and the equivalent surface area that the deposit covers; the calculation must also evaluate the deposit porosity.

As stated earlier, inlet and outlet water samples show that the fouling mechanism for Test 1 (city water) was crystallization alone while that for Test 2 (river water) involved only particulate fouling. Visual indication of the fouling layer of the tubes (Fig. 6), as well as the inlet/outlet sample testing, confirm this identification of the fouling mechanisms.

Tube Inspection

Each tube that undergoes fouling is cut open and analyzed. Visual inspection along with microscope scans allows determination of surface area coverage, deposit thickness, and deposit roughness. In Figure 6,tubes from Test 2 with river water are shown along with a sample of roughness and deposit height from the microscope.

Figure 6 (a) – (c) shows each half of the two test sections, where the two leftmost tubes and rightmost tubes in each picture belong to the 1 m/s and 2 m/s tube, respectively. This fouling layer is particulate, with chemical analysis of the river water showing no propensity for crystallization and a substantial amount of suspended solids in the water. At the inlet (a) and outlet (c) sections, the non-heated length before the test section shows little to no deposit, indicating that higher interface temperature increases fouling deposition rate for particulates. Secondly, visual inspection shows a clear trend of lighter-to-darker deposit when moving from figures (a) through (c), from inlet to outlet. The darker deposit is thicker—even in particulate fouling, the fouling layer does not disperse evenly, but distributes according to the higher-interface temperature at the outlet of the tube.

The microscope scan was performed over a section of the middle tube, shown by the red box in Figure 6 (b). The deposit was physically scraped away and a scan was performed over the tube section. Figure 6 (d) shows the height profile of the scan. In this figure, the scraped surface is seen from around 7500 to 12500 microns in the X-distance. This section exhibits a much lower roughness value and is 10 – 20 microns lower than the rest of the scan. Even this thin fouling deposit increases tube roughness, despite being only 10 – 20 microns thick.

The differences between the 1 and 2 m/s velocities are apparent as well. Note that the left two halves in each image are the 1 m/s tubes, and the right two halves are the 2 m/s tubes. At the inlet (a) and outlet (c) there is a thicker deposit for the 1 m/s tube before the heated section than that of the 2 m/s tube.

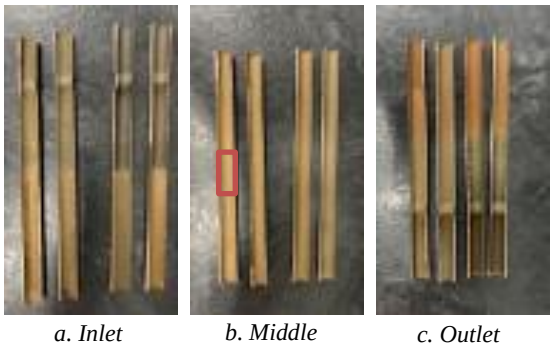

a. Inlet *b. Middle* *c. Outlet*

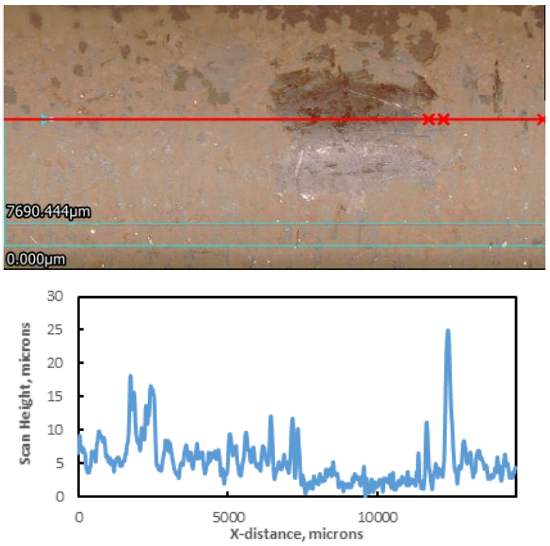

d. Height measurement and optical test – middle

Fig 6. Tube section pictures (a,b,c) at entrance, middle, and exit of test section along with tube scan and height profile (d)

In reviewing fouling resistance, pressure drop trends, physical observations, and microscope scans, a picture of high-quality data from HTRI's cooling water fouling unit emerges. Comparison between fouling thermal and hydraulic resistance, fouling layer coverage, thickness, roughness, and water chemistry allows a full evaluation of the fouling process. The data from the unit is applicable to fouling performance comparison as well as fouling research.

DATA ANALYSIS

Most mathematical descriptions of cooling fouling start with some form of the well-known Kern-Seaton model [6], where the change in fouling layer mass or thickness over time is postulated as a function of deposition and removal.

ISBN: 978-0-9984188-3-4; Published online www.heatexchanger-fouling.com

$$\frac{dm}{dt} = \Phi_d - \Phi_r \tag{9}$$

This equation predicts that a fouling layer builds up until the shear removal rate equals the deposition rate. Fouling layer buildup increases pressure drop by constricting flow and increasing roughness, which increases the shear on the surface of the deposit. This shear increase then raises the removal rate of the deposit, according to the Kern-Seaton model [7].

The Kern-Seaton model does not incorporate several items apparent from fouling literature as well as new HTRI data. First, the effects of roughness are not quantified. Roughness absolutely affects both friction factor and heat transfer, meaning that a mass deposition rate can have different effects depending on the distribution of that mass over the tube. Note Test 2 pressure drop and heat transfer trends—the changing layer porosity and roughness affects the pressure drop and heat transfer differently. HTRI's data analysis includes properly calculating the friction factor change throughout the fouling process.

We calculate the friction factor by measuring the pressure drop of the tube. This same friction factor is then applied for the pressure drop under a steadily increasing fouling layer and decreasing flow area. (The fouling layer is assumed to have uniform thickness and full area coverage). A very thick 600-micron fouling layer thickness is used as the upper bound. Applying this thickness to the entire tube length results in an increase in pressure drop with a constant roughness, as shown in Fig. 7.

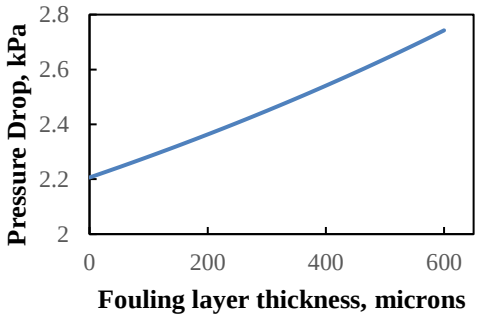

Fig. 7. Pressure drop due to constriction.

These thickness values shown in Fig. 7 can be compared to an assumed thermal conductivity of the fouling layer of 2.8 W/m K [1]. This is close to the thermal conductivity of calcite and clay sediments suspended in the river water. Assuming complete surface area coverage, zero porosity, and congruent layer thickness, the thermal resistance of a foulant layer can be calculated for these thicknesses using Equation (7). However, as most fouling layers are porous, the thermal conductivity of water must be considered as well. Fig. 8 shows a maximum and minimum thermal fouling resistance as the fouling layer varies between 0% and 100% porosity. The thermal fouling resistance of the blue line assumes the foulant as the only additional thermal resistance, whereas the red line assumes water as the only additional thermal resistance. Note that water's lower thermal conductivity allows a much greater thermal fouling resistance, indicating that the porosity of the fouling layer may impact the thermal resistance to a greater extent than the thickness of the fouling layer. A thin, highly porous fouling layer can cause greater thermal resistance than a thick, solid thermally conductive fouling layer.

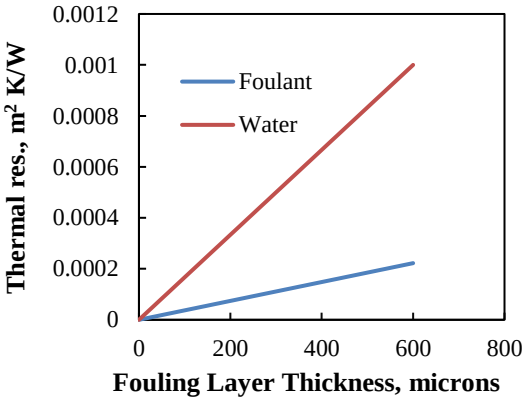

Fig. 8. Stationary water vs. foulant thermal resistance.

The actual fouling layer thickness of Test 2 is shown by microscope scans, such as those shown in Fig. 6. A portion of the fouling layer was physically removed in the scan to help estimate the fouling layer thickness. Fig. 5 shows the results of the fouling layer thickness measurement on the middle of the 1 m/s tube of Test 2, with only particulate fouling occurring. The typical fouling layer thickness is around 10 – 15 microns, with an upper limit around 25 microns and certain parts of the fouling layer as thick as 20 microns. These measurements are not as thick as Fig. 7 and Fig. 8 might indicate, where a thickness of 20 microns would result in a constriction pressure drop increase of only 0.02 kPa. Assuming the thermal conductivity of the fouling layer is similar to that of water, a thermal fouling resistance of 3.45E-5 W/m^2 K is estimated. In Test 2, the asymptotic fouling resistance was around 4.5E-5 W/m^2 K with a pressure drop increase of 0.4 kPa. A discrepancy exists here that has several possible explanations.

These results show the value of microscope scans, surface area coverage, and visual observation of fouling deposits in interpreting data. Deposit roughness plays a role in the changing friction factor and thermal resistance, and continued HTRI research seeks to establish exactly what that role is. Additionally, regarding particulate fouling, it is expected that the fouling deposits contain a high amount of water, dropping the thermal conductivity

ISBN: 978-0-9984188-3-4; Published online www.heatexchanger-fouling.com

below that of a non-porous deposit. Bloating and expansion of the fouling layer due to water saturation may play a role as well, as measurements are taken with dried tubes.

DISCUSSION

The Moody chart (Fig. 9) provides a starting point in understanding how the fouling layer affects the roughness and pressure drop of the flow inside a tube.

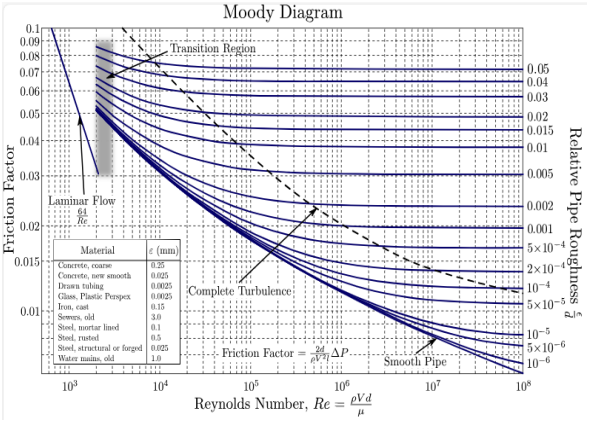

Fig. 9. Moody chart [8]

This chart highlights the effects of relative pipe roughness on the friction factor. When fouling occurs, the roughness of the pipe changes, changing the friction factor. However, as is well-known, this increasing roughness has an effect only at the point at which the flow "feels" the roughness [9]. This point can be determined by calculating the sublayer thickness. This sublayer thickness is calculated using the concept of "friction velocity", and is equivalent to

$$\mu^* = \sqrt{\frac{\tau_w}{\rho}} \tag{10}$$

$$\delta_{vel} = C\frac{\mu}{\mu^*\rho} \tag{11}$$

In most cases, C is taken to be equal to 5.0 [9].

These calculations allow us to estimate at what point the fouling layer height begins to affect the friction factor, an effect which is noticeable in the pressure drop data of Test 2. Combined with microscope scans, a determination of the final friction factor is linked to the fouling layer roughness and thickness.

Hydraulic and thermal performance quantification requires a total analysis of the data available. Thickness and roughness must be measured, and the connection to pressure drop and friction factor allows us an understanding of the total fouling layer effect on hydraulic trends.

HTRI's goal is to understand the processes that lead to buildup of the fouling layer and correctly quantify the effects this fouling layer will have on both hydraulic and thermal performance. Hydraulically, constriction and roughness increase pressure drop, so the research process establishes the link between the deposit roughness and the friction factor. Deposit thermal conductivity and thickness directly affect the heat transfer resistance. Data shows this thermal conductivity must consider deposit porosity.

CONCLUSION

This paper has introduced HTRI's cooling water fouling rig, described the rig's design and capabilities, highlighted the data analysis process, presented a portion of the test data, and discussed analysis methods that provide additional insight into the data and fouling deposit effects. This information is pertinent in evaluating tube coatings, enhancements, metallurgies, and mitigation methods testing currently planned on the HTRI cooling water fouling rig. A total performance and comparison is available with the steps outlined here.

Most fouling research has been tied to the Kern-Seaton model, which assumes thermal resistance to be equivalent to that of the fouling layer thickness but does not consider surface area coverage, porosity of the fouling layer, or deposit roughness. Continuing HTRI research will fully investigate these parameters, especially in tube performance comparison of the cooling water fouling unit.

It is difficult to reconcile hydraulic and thermal resistance increases due to fouling deposits. More understanding will be gained if the effects of surface area coverage, porosity, and roughness are included to interpret data according to the techniques presented in this paper. Additionally, the hydraulic effects of fouling are rarely considered in literature beyond constriction. The data presented here clearly illustrate the effects of roughness on pressure drop, which outweigh the drop in thermal performance in Test 2.

NOMENCLATURE

A Area, m^2
a Coefficient
b Coefficient
C Coefficient
h Heat transfer coefficient, W/m^2 K
k Thermal conductivity, W/m K
$LMTD$ Log Mean Temperature Difference, K
m Mass, kg
n Coefficient
Nu Nusselt number, dimensionless
Pr Prandtl number, dimensionless
Q Duty, W
R Thermal resistance, m^{2}K/W
Re Reynolds number, dimensionless
T Temperature, °C
t Time, s

ISBN: 978-0-9984188-3-4; Published online www.heatexchanger-fouling.com

U Overall heat transfer coefficient, W/m^{2}K
δ Thickness, m
μ Viscosity, Pa-s
μ^* Friction velocity, m/s
ρ Density, kg/m^3
τ Shear, Pa
Φ Rate, kg/s

Subscript
avg average
clean clean
d deposit
f fouled
i inner
initial initial
o outer
r removal
s shell
t tube
u uncorrected
vel velocity
w wall

REFERENCES

[1] ESDU Oil Industry Fouling Working Party, Fouling in cooling systems using fresh water, ed. D. C. King, 58, IHS (1998).

[2] A. Ganguli, Heat transfer correlations for intube turbulent flow of liquids and gases, S-ST-1-1, Heat Transfer Research, Inc., Navasota, TX (1981).

[3] W. Augustin, S. Scholl, and F. Schluter, Introducing a holistic approach to model and link fouling resistances, *Heat Mass Transfer* **57**, 999-1009 (2021).

[4] F. Schluter, W. Augustin, and S. Scholl, Application of experimental data to model local fouling resistances, *Heat Mass Transfer* **58**, 29-40 (2021).

[5] F. Schlüter, W. Augustin, and S. Scholl, Experimental study of local crystallization fouling in double-pipe heat exchangers, F-EX-1-14, Heat Transfer Research, Inc., Navasota, TX (2019).

[6] T. R. Bott, *Fouling of Heat Exchangers*, ed. T. R. Bott, 23, Elsevier Science, Amsterdam, The Netherlands (1995).

[7] E. M. Ishiyama, W. R. Paterson, and D. I. Wilson, The effect of fouling on heat transfer, pressure drop and throughput in refinery preheat trains: Optimisation of cleaning schedules, in *Proc. 7th Intl. Conf. on Heat Exchanger Fouling and Cleaning – Challenges and Opportunities*, vol. RP5, eds. H. Müller-Steinhagen, M. R. Malayeri, and A. P. Watkinson, 47 – 56, Berkeley Electronic Press (2007).

[8] S. Beck and R. Collins, University of Sheffield, Moody diagram, (Donebythesecondlaw at English Wikipedia), conversion to SVG: Marc.derumaux, CC BY-SA 4.0, https://creativecommons.org/licenses/by-sa/4.0, via Wikimedia Commons (2016). https://commons.wikimedia.org/wiki/File:Moody_EN.svg

[9] B. R. Munson, T. H. Okiishi, W. W. Huebsch, and A. Rothmayer, *Fundamentals of Fluid Mechanics*, ed. J. Welter, 7th ed., 418-424, John Wiley & Sons, Hoboken, NJ, USA (2013).

ISBN: 978-0-9984188-3-4; Published online www.heatexchanger-fouling.com